

# Non-orthogonal spin-momentum locking

T. Hakioglu <sup>†, 1, 2, \*</sup> Wei-Chi Chiu,<sup>2, †</sup> R. S. Markiewicz,<sup>2</sup> Bahadur Singh,<sup>3</sup> and A. Bansil<sup>2</sup>

<sup>1</sup>*Energy Institute and Department of Physics, Istanbul Technical University  
Maslak 34469, Istanbul, Turkey*

<sup>2</sup>*Department of Physics, Northeastern University, Boston, MA 02115, USA*

<sup>3</sup>*Department of Condensed Matter Physics and Materials Science,  
Tata Institute of Fundamental Research, Colaba, Mumbai 400005, India*

Spin-momentum locking is a unique feature of spin-orbit coupled materials and a key to their promise of applications in spintronics and quantum computation. Much of the existing work has been focused on an orthogonal locking between the directions of spin and momentum vectors in the context of both topological and non-topological materials. Mechanisms responsible for non-orthogonal spin-momentum locking (NOSML) have drawn little attention, although an NOSML effect has been reported on the topological surface of  $\alpha$ -Sn. Here, we demonstrate how spin-orbit scattering from non-magnetic impurities can produce the NOSML state. The parameter describing spin-orbit coupling strength in our analysis of the NOSML could be extracted directly from the spin-resolved angle-resolved photoemission (S-ARPES) spectra. Our formalism is applicable to all spin-orbit coupled systems and not limited only to topological states. An understanding of NOSML effects bears on spin-orbit dependent phenomena more generally, including issues of spin-to-charge conversion and the interpretation of quasiparticle interference (QPI) patterns and scanning-tunneling spectra (STS) in materials.

Spin-momentum locking (SML) occurs commonly in spin-orbit coupled materials with or without topological bands[1–4]. Its telltale signature involve forbidden backscattering [5, 6] from non-magnetic impurities (no ‘U-turn’) and enhancement of weak antilocalization effects [7]. SML enables electrical control of spin polarization in nonequilibrium transport and thus plays a key role in spintronics and spin-based quantum information sciences applications [2, 8] by driving the presence of a spin-polarized component of current with polarization perpendicular to the current density [9–11].

The orthogonal SML (OSML)—see Fig.1.a, is common in materials exhibiting SML[1–3]. The OSML state is the result of in-plane Rashba spin-orbit coupling (SOC) observed first time on the Au/Ge(111) surface long before the topological materials were discovered[12]. In topological insulators, OSML with a  $\pi$ -Berry phase is an essential feature of the surface state[13]. It has been utilized in the electrical detection of magnon decay[14]. An S-ARPES study of the Au/Ge(111) surface revealed weak anisotropic violations from orthogonality[15] and similar effects have been reported in high-temperature superconductors[16]. As an example of the topological insulators, in  $Bi_{2-y}Sb_yTe_xSe_{3-x}$  compounds the spin-momentum angle at the Fermi surface is weakly unlocked anisotropically (Fig.1.b)[17]. High-order corrections to the  $\mathbf{k}\cdot\mathbf{p}$  Hamiltonian have been shown to induce deviations from the orthogonal picture[18]. Many body interactions can also cause similar effects as the electron-phonon interaction [19–22] was recently studied in this context[23, 24].

Another type of deviation from perfect orthogonality is the NOSML as illustrated in Figs.1.c and d. Such a state has been reported on the topological surface of

strained  $\alpha$ -Sn [25, 26]. Here, S-ARPES and Mott polarimetry reveal the presence of a radial component of the spin (Fig.1.c) with a significant inward deviation of  $\Phi_0 - 90^\circ \simeq 20^\circ$  on a circular Fermi surface. The out-of-plane spin  $S_z$  is observed to vanish conforming with the absence of the out-of-plane SOC along with even rotational symmetry. Note that  $\alpha$ -Sn is inversion symmetric in unstrained and strained phases [26–33]. Ref.[25] also suggests the presence of electron-impurity interaction through an analysis of the imaginary part of the electronic self-energy.

The last observation is of key importance in our theory of the NOSML. Our approach is not limited to topological surface states but addresses NOSML as a general phenomenon in materials with strong SOC. The presence of inversion and time-reversal symmetries substantially constrains the Hamiltonian for treating non-interacting bands. Origin of the NOSML lies beyond the realm of warped electronic bands and details of the lattice structure are not important for generating this effect.

## THE THEORY OF INTERACTING SPIN

Our starting point is the time-reversal invariant Hamiltonian in the pseudo-spin  $|\mathbf{k}\sigma\rangle$  basis ( $\hbar = 1$ )[1, 34, 35]:

$$\mathcal{H}_0 = (\xi_{\mathbf{k}} - \mu)\sigma_0 + \mathbf{g}_{\mathbf{k}} \cdot \boldsymbol{\sigma} \quad (1)$$

where  $\boldsymbol{\sigma} = (\sigma_x, \sigma_y, \sigma_z)$  is the pseudo spin representing the spin-orbit coupled total angular momentum states[1],  $\mathbf{k} = (k_x, k_y) = k(\cos\phi_{\mathbf{k}}, \sin\phi_{\mathbf{k}})$  is the electron wavevector relative to the Dirac point at  $\mathbf{k} = 0$  and  $\xi_{\mathbf{k}}$  and  $\mu$  are the spin-independent bare electron band and the chemical potential, respectively. The Hamiltonian in Eq.(1) is the most basic Hamiltonian that can capture

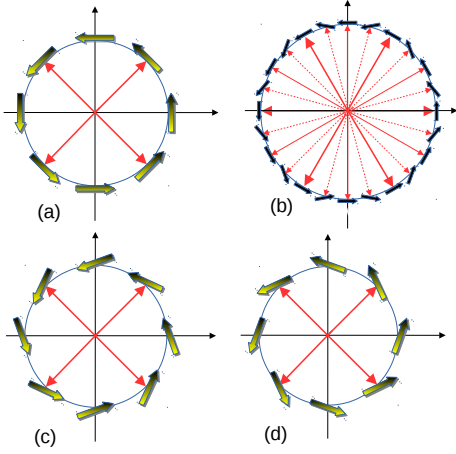


FIG. 1. A schematic of various planar spin-momentum locking cases for a chiral band. (a) The OSML. (b) Weakly unlocked case of  $Bi_2Se_3$  and  $Bi_2Te_3$ . The weak out-of-plane component is not shown. (c, d) NOSML with  $\delta < 0$  (c) and  $\delta > 0$  (d).  $\delta$  is defined in Eq.(16).

surface states in a strong topological insulator. A pair of such Hamiltonians can be used to model states in Dirac and Weyl semimetals as well as Rashba type interface states. The spin-orbit vector  $\mathbf{g}_k$  is normally composed of an in-plane component  $\mathbf{g}_{\parallel k} = g_0 \hat{z} \times \mathbf{k}$  with  $g_0$  as the Rashba type in-plane SOC and  $\hat{z}$  as the surface unit normal vector, and an anisotropic out-of-plane  $\mathbf{g}_{\perp k}$  component. The general spin-orbit eigenstates  $|\mathbf{k}\lambda\rangle$  of Eq.(1), where  $\lambda = \pm$  describes the spin-orbit band index, include the chiral spin-1/2 state not only attached to the dominant  $|p_z\rangle$  orbitals as considered conventionally, but also the in-plane orbitals  $|p_x\rangle$  and  $|p_y\rangle$ . The role played by the in-plane orbitals is strongly material dependent, which has been demonstrated experimentally[36] and theoretically[37]. The observed pseudospin in these free bands is given by  $\langle \mathbf{J} \rangle = \langle \mathbf{k}\lambda | \boldsymbol{\sigma} | \mathbf{k}\lambda \rangle = (\lambda/2) \hat{\mathbf{g}}_k$ , where  $\hat{\mathbf{g}}_k$  is the unit spin-orbit vector, which coincides with the actual spin  $\mathbf{S}^\lambda(\mathbf{k}) = (\lambda/2) \hat{\mathbf{g}}_k$  and the OSML follows from  $\hat{\mathbf{g}}_k \cdot \mathbf{k} = 0$ .

The Eq.(1) is clearly insufficient to describe all strongly spin-orbit coupled surfaces and additional terms are allowed by symmetry. For instance, the cubic Dresselhaus SOC is present in the absence of inversion symmetry in ordinary semiconductors[1]. Its realization in  $Bi_2X_3$  type strong topological insulators results in the hexagonal warped Fermi surfaces[38]. Note that since NOSML is an isotropic effect, anisotropic warping effects in the band structure can hinder its observation. Therefore, we ignore the warping anisotropy and examine symmetry allowed Hamiltonians which can lead to the NOSML state. We thus arrive at the minimal Hamiltonian[1, 34, 35]

$$\mathcal{H}_1 = \gamma \mathbf{k} \cdot \boldsymbol{\sigma} \quad (2)$$

A term of the form in Eq.(2) is present in the Kane

model between the  $\Gamma_{7c}$  and  $\Gamma_{6c}$  bands of zinc-blende structures[1, 39, 40]. The total Hamiltonian  $\mathcal{H}_0 + \mathcal{H}_1$  is equivalent to  $\mathcal{H}_0$  by the mapping  $g_0 \rightarrow g_0 + i\gamma$ . The energy spectrum is linear and spin-momentum are locked non-orthogonally at  $\Phi_0 = \pm(\pi/2 + \tan^{-1}\gamma/g_0)$  with the  $\pm$  describing the upper and the lower Dirac cones. While, Eq.(2) can easily accommodate a non-orthogonal state of the spin and momentum in zinc-blende structures[40], it is not applicable when the inversion symmetry holds since then it is required that  $\gamma = 0$ . This prompts us to think that the NOSML in inversion symmetric systems may have its origin fundamentally beyond the class of symmetry allowed single particle Hamiltonians.

Here, the observation of the electron-impurity interaction on the circularly symmetric Fermi surface of  $\alpha$ - $Sn$ [25] may provide a striking clue for the general source of the NOSML. It is known that the electron-impurity interaction, combined with the strong SOC, gives rise to the spin-orbit scattering in addition to the scalar scattering channels, which then leads to a number of observable transport phenomena. These are linearly dependent on the spin-orbit scattering strength[41] such as corrections in the momentum and spin relaxation, spin-dependent diffusion, weak localization/antilocalization[2] and anomalous spin-texture[42]. The spin-orbit scattering between the impurity and the electron bands also provides a platform for NOSML and this is the main focus of this work.

We consider the Green's function for renormalized spin under interactions [24]:

$$\mathbf{S}^\lambda(\mathbf{k}) = \frac{\lambda}{2} \hat{\mathbf{G}}(\mathbf{K}^*) \quad (3)$$

and apply it to the electron-impurity interaction. Here, the  $*$  indicates that  $\mathbf{S}^\lambda(\mathbf{k})$  is calculated at the physical pole position  $E^* = E_k^\lambda$  of the full Green's function[24].  $\mathbf{G}(\mathbf{K}^*) = \mathbf{g}_k + \boldsymbol{\Sigma}(\mathbf{K}^*)$ , with  $\mathbf{K}^* = (\mathbf{k}, iE^*)$  in the Matsubara Green's function formalism, is the renormalized spin-orbit vector,  $\hat{\mathbf{G}}^* = \mathbf{G}^*/|\mathbf{G}^*|$  is its unit vector, and the  $\boldsymbol{\Sigma}(\mathbf{K}^*)$  is the impurity averaged and spin-dependent-self-energy (SDSE) defined below. The full self-energy is defined by the matrix

$$\boldsymbol{\Sigma}(\mathbf{K}) = \Sigma_0(\mathbf{K})\sigma_0 + \boldsymbol{\Sigma}(\mathbf{K}) \cdot \boldsymbol{\sigma} \quad (4)$$

where  $\Sigma_0$  is the spin neutral self-energy (SNSE) and  $\boldsymbol{\Sigma} = (\Sigma_x, \Sigma_y, \Sigma_z)$  is the SDSE. The total change in the spin due to this interaction in the electron band  $\lambda$  is given by  $\Delta \mathbf{S}^\lambda(\mathbf{k}) = (\lambda/2) [\hat{\mathbf{G}}^*(\mathbf{k}) - \hat{\mathbf{g}}_k]$ . In the weak interaction limit[24] this takes a suggestive form with the leading term

$$\Delta \mathbf{S}_{\parallel}^\lambda(\mathbf{k}) \simeq \frac{\lambda}{2} \frac{\Sigma_k^*}{|\mathbf{g}_k|} \hat{\mathbf{k}} \quad (5)$$

where  $\Sigma_k^* = \boldsymbol{\Sigma}(\mathbf{K}^*) \cdot \hat{\mathbf{k}}$  is the component of the SDSE along the momentum. The Eq.(5) states that the interactions can change the orthogonality of the spin and momentum by inducing a finite  $\Sigma_k^*$ .

## THE SPIN-ORBIT IMPURITY SCATTERING

It is clear that the formalism in Eqs. (3-5) hinges upon an accurate interaction model for the self-energy in Eq.(4). In our model here, the electron-impurity interaction  $V_{ei}^{(i)} = V_0^{(i)} + V_{so}^{(i)}$  has spin-independent part  $V_0^{(i)}$  and a spin-orbit scattering part  $V_{so}^{(i)}$  and  $i$  refers to the  $i$ 'th impurity. The spin-orbit coupling within the electron band is assumed to be sufficiently strong whereas the interaction of the electron and the impurity is weak. This enables a perturbative treatment of the electron-impurity interaction within each spin-orbit band  $\lambda$  where the energetically unfavorable interband mixing can be neglected. The intraband scattering matrix between the initial and final states  $|i\rangle = |\mathbf{k}\lambda\rangle$  and  $|f\rangle = |\mathbf{k}'\lambda\rangle$  is  $T_{\mathbf{k},\mathbf{k}'}^{\lambda,\lambda} = \sum_i \langle \mathbf{k}'\lambda | V_{ei}^{(i)} | \mathbf{k}\lambda \rangle = T_{0\lambda}(\mathbf{k}, \mathbf{k}')$  as given in[2, 41, 43–53] and [54] by,

$$T_{0\lambda}(\mathbf{k}, \mathbf{k}') = \sum_i e^{i(\mathbf{k}-\mathbf{k}') \cdot \mathbf{R}_i} t_{0\lambda}^{(i)}(\mathbf{k}, \mathbf{k}') \quad (6)$$

where the exponential phase factor accounts for the impurity scattering phase shifts occurring at random centers  $\mathbf{R}_i$  and  $t_{0\lambda}^{(i)}(\mathbf{k}, \mathbf{k}')$  is the scattering amplitude of the electrons which can be derived microscopically once the impurity-electron scattering potential is known. We will assume that there is only one kind of impurity and drop the  $i$  index from  $t_{0\lambda}^{(i)}$ . We then write it as a sum of even and odd contributions under the exchange of initial-final scattering states as[54]

$$t_{0\lambda}(\mathbf{k}, \mathbf{k}') = a + b \hat{\mathbf{k}} \cdot \hat{\mathbf{k}}' + c \hat{\mathbf{k}} \times \hat{\mathbf{k}}' \cdot \hat{\mathbf{z}}. \quad (7)$$

Here,  $a, b, c$  are complex coefficients describing the  $s$ -wave,  $p$ -wave and the spin-orbit scattering strengths[48] and generally depend on  $\mathbf{k}$  and  $\mathbf{k}'$ . They are strongly material dependent via the impurity-electron potential and the spin-orbital states  $|\mathbf{k}\lambda\rangle$  [2, 47–50]. We further consider dilute impurity limit  $n_i \ll \lambda_F^{-3}$  where  $n_i$  is the impurity concentration and  $\lambda_F$  is the Fermi wavelength.

## THE SELF-ENERGY DUE TO THE SPIN-ORBIT SCATTERING

### The spin-independent self-energy

The full self-energy in Eq.(4) can be written as the sum of contributions from each spin-orbit band as  $\underline{\Sigma}(\mathbf{K}) = \sum_{\lambda} \underline{\Sigma}^{(\lambda)}(\mathbf{K})$  where[43, 44, 55] the self-energy in the  $\lambda$  band can be defined as

$$\begin{aligned} \underline{\Sigma}^{(\lambda)}(\mathbf{K}) &= \frac{n_i}{2} \int \frac{d\mathbf{k}'}{(2\pi)^2} \\ &\times |t_{0\lambda}(\mathbf{k}, \mathbf{k}')|^2 [1 + \lambda \hat{\mathbf{G}}(\mathbf{k}', E) \cdot \boldsymbol{\sigma}] \mathcal{G}^{\lambda}(\mathbf{k}', E) \end{aligned} \quad (8)$$

The  $\mathcal{G}^{\lambda}(\mathbf{k}, E) = 1/(E - E_{\mathbf{k}}^{\lambda})$  is the Green's function of the eigenband with index  $\lambda$  and  $E_{\mathbf{k}}^{\lambda} = \tilde{\xi}_{\mathbf{k}} + \lambda |\mathbf{G}^{\lambda}(\mathbf{k}, E)|$

as the renormalized energy band with  $\tilde{\xi}_{\mathbf{k}}^{\lambda} = \xi_{\mathbf{k}} + \Sigma_0^{(\lambda)}$  and  $\mathbf{G}^{\lambda} = \mathbf{g}_{\mathbf{k}} + \underline{\Sigma}^{(\lambda)}$ . The  $n_i$  dependence in Eq.(8) comes from the averaging over the random impurity positions  $\mathbf{R}_i$  as given in Eq.(6) as shown in the supplementary material. These equations can also be obtained from our earlier theory in the elastic limit[24].

The NOSML is fundamentally an isotropic effect which could be concealed by warping anisotropy. We therefore confine our work to the case when such phenomena are absent or sufficiently weak and consider an isotropic band  $\xi_{\mathbf{k}}^{\lambda} = \hbar^2 k^2/(2m) + \lambda g_0 k$ . The SNSE and the SDSE in the Eq.(8) are extracted as

$$\Sigma_0 = \text{Tr}\{\underline{\Sigma}\}/2, \quad \underline{\Sigma} = \text{Tr}\{\underline{\Sigma} \boldsymbol{\sigma}\}/2 \quad (9)$$

Assuming that the  $p$ -wave and the spin-orbit scattering strengths are negligibly small compared to that of the  $s$ -wave, i.e.  $|b| \ll |a|$  and  $|c| \ll |a|$ , the  $s$ -wave scattering strength can be related to the spin-independent self-energy  $\Sigma_0$ . Using the Eq's.(9) we have,

$$\text{Im } \Sigma_0^{\lambda}(E) \simeq \frac{m}{4\hbar^2} n_i |a|^2 \left( 1 - \frac{g_0}{\sqrt{g_0^2 + \frac{2\hbar^2}{m} E}} \right). \quad (10)$$

The  $\text{Im } \Sigma_0^{\lambda}(E)$  can be inferred from the quasiparticle momentum distribution curves[25], which can then be used to extract the  $n_i |a|^2$  phenomenologically.

### The spin-dependent self-energy and the NOSML

We now turn to the spin-dependent component  $\underline{\Sigma}$  in Eq.(8), which can be extracted by using the second of the Eqs.(9). Note that  $\mathbf{g}_{\mathbf{z}\mathbf{k}}$  and  $\Sigma_z$  are both absent here due to the manifest rotational symmetry. We can therefore write  $\underline{\Sigma} = (\Sigma_x, \Sigma_y, 0)$  in the polar form as

$$\underline{\Sigma} = \Sigma_g \hat{\mathbf{g}}_{\parallel\mathbf{k}} + \Sigma_k \hat{\mathbf{k}} \quad (11)$$

where we define  $\Sigma_g = \underline{\Sigma} \cdot \hat{\mathbf{g}}_{\parallel\mathbf{k}}$  and  $\Sigma_k = \underline{\Sigma} \cdot \hat{\mathbf{k}}$  as the scalar components of  $\underline{\Sigma}$  along the  $\hat{\mathbf{g}}_{\parallel\mathbf{k}}$  and  $\hat{\mathbf{k}}$  directions. This form of  $\underline{\Sigma}$  is particularly useful in the impurity averaging of the SDSE, as  $\Sigma_g$  and  $\Sigma_k$  are invariant functions under rotations in  $\mathbf{k}$ -space, a useful concept considering the random momentum directions in each scattering event. Eq.(11) is equivalently written as

$$\Sigma_x - i \Sigma_y = e^{-i(\phi + \pi/2)} \mathcal{S}_k \quad (12)$$

where  $\mathcal{S}_k = \Sigma_g + i \Sigma_k$  is an even complex function. The  $\Sigma_g = \text{Re}\{\mathcal{S}_k\}$  renormalizes the spin-orbit strength by  $g_0 \rightarrow g_0 + \Sigma_g/k$ . It can be ignored if  $g_0 k$  is sufficiently strong. The  $\Sigma_k = \text{Im}\{\mathcal{S}_k\}$ , on the other hand, is an emerging component which is the main cause of the change in the spin-momentum locking angle in Eq.(5) and which must be found from the spin-dependent part of Eq.(8). Using Eq.(12) in Eq.(8) we find

$$\mathcal{S}_k^{\lambda} = \lambda \frac{2\hbar^2}{m} (\text{Im } \Sigma_0) \int \frac{k' dk'}{2\pi} T_{0\lambda}(k, k') \mathbb{S}^{\lambda}(k') \quad (13)$$

where

$$\mathcal{T}_{0\lambda}(k, k') = \frac{1}{|a|^2} \int \frac{d\theta_{\mathbf{k}, \mathbf{k}'}^2}{2\pi} \left| t_{0\lambda}(\mathbf{k}, \mathbf{k}') \right|^2 e^{-i\theta_{\mathbf{k}, \mathbf{k}'}} \quad (14)$$

It is easily shown using Eq.(7) in Eq.(14) that (see the Supplementary Material) that  $\mathcal{T}_{0\lambda} = (1 + \text{Re}\{ab^*\})/|a|^2 - i\text{Re}\{ac^*\})/|a|^2$ . The  $\mathbb{S}^\lambda(k)$  is given by

$$\mathbb{S}^\lambda(k) = \frac{g_k + \mathcal{S}_k^\lambda}{|\mathbf{G}^\lambda(k, E)|} \frac{1}{E - E_k^\lambda} \quad (15)$$

Eq.(13) is the complex-scalar equivalent of the matrix equation in Eq.(8). This scalar property is crucial in enabling the impurity average by essentially eliminating the effect of the randomness in the momentum orientations and bringing each impurity scattering on an equal footing. In order to make a connection with the spin-texture measurements, we now define a microscopic spin-deviation angle  $\delta_k^\lambda$  as shown in the Fig.(2). The  $\delta_k^\lambda$  is related to the imaginary part  $\bar{c} = \text{Re}\{ac^*\}/|a|^2$  of the  $\mathcal{T}_{0\lambda}$ . Using the geometry in the Fig.2 we write[17, 23, 24]

$$\sin \delta_k^\lambda = \frac{\mathbf{S}_{\parallel k} \cdot \hat{\mathbf{k}}}{|\mathbf{S}_{\parallel k}|} \rightarrow \frac{\Sigma_k^\lambda}{|\mathbf{G}_k|} \quad (16)$$

The two cases identified in Fig.2 as  $\delta_k^\lambda < 0$  and  $\delta_k^\lambda > 0$  are determined by the sign of the imaginary part of  $\mathcal{T}_{0\lambda}$ . In order to proceed at a microscopic level, the coefficients of the scattering amplitude  $t_0(\mathbf{k}, \mathbf{k}')$  in Eq.(7) must be known. Here we consider  $\bar{c} = \text{Re}\{ac^*\}/|a|^2$  as a parameter and simply assume that  $a = 1$ . The calculated  $\delta_k^\lambda$  at the Fermi level is shown for the + band in Fig.3 as  $\bar{c}$  and  $\alpha = \text{Im} \Sigma_0/E_F$  are varied. It is easy to see that  $\delta_k^\lambda$  vanishes linearly with  $\bar{c}$  and has a steep behavior in the vicinity of  $\bar{c} = 0$ . For  $\bar{c} \neq 0$ , the inward/outward tilt of the spin is decided by the sign of  $\bar{c}$ . Eqs.(3) and (13) also predict that the anomalous component of the spin along the momentum in the upper and lower Dirac cones are opposite to each other. The component of the spin originating directly from the spin-orbit vector  $\mathbf{g}_k$  is linearly

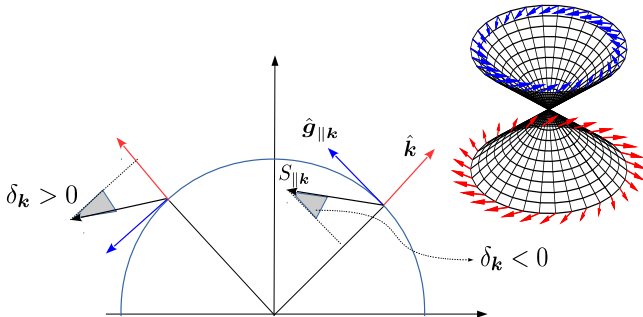


FIG. 2. Spin deviation angle  $\delta_k^\lambda$  is illustrated for two different cases  $\delta_k^\lambda < 0$  and  $\delta_k^\lambda > 0$ . The  $\delta_k^\lambda$  has the same sign in the upper and lower Dirac cones which is shown for the  $\delta_k^\lambda > 0$  case in the inset.

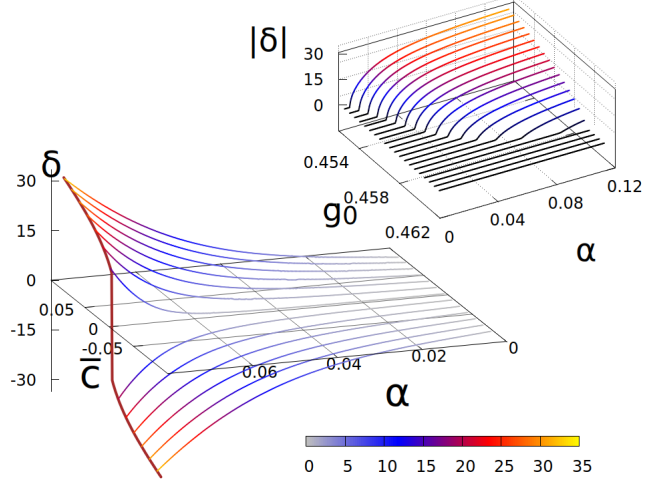


FIG. 3. The  $\delta_k^\lambda$  (in degrees) at the Fermi surface for the  $\lambda = +$  band in Eq.(16) using the Eq.(13) as the spin-orbit scattering amplitude  $c$  and the  $\alpha$  are varied. The inset at the top right depicts at  $c = 0$  the behaviour near the sharp boundary between the OSML ( $\delta = 0$ ) and the NOSML ( $\delta \neq 0$ ) phases as a function of  $\bar{g}_0 = g_0 k_F/E_F$  and  $\alpha = \text{Im} \Sigma_0/E_F$ . The color scale is for the  $|\delta_k^\lambda|$  and applies to both plots. We used  $k_F = 0.035 \text{ Å}^{-1}$  and  $E_F = 150 \text{ meV}$  for the normalization[25].

dependent on  $\lambda$  as shown by Eq.(3) while the self-energy contribution has a  $\lambda^2$  pre-factor. Additionally, one must consider the  $E$  dependence in Eq.(13) at the physical pole position  $E = E_k^\lambda$ . The  $\Sigma_k$  changes sign as the upper Dirac cone with  $E = E_k^+$ ,  $\lambda = +$  is changed to the lower Dirac cone with  $E = E_k^- = -E_k^+$ ,  $\lambda = -$ . The combined effect of these is that  $\mathbf{S}_k^\lambda$  has opposite signs in the upper and lower Dirac cones (as shown in the inset of Fig.2).

## DISCUSSION AND CONCLUSION

An important point here is that under the strong spin-orbit coupling the spin and the angular momentum vectors are not individually conserved but the total angular momentum  $\mathbf{J} = \mathbf{L} + \mathbf{S}$  is. This leads to the formation of the orbital texture in which the orbital configurations can affect the spin texture[36, 37]. The dominant bands are usually  $|p_z\rangle$ -like out-of-plane orbitals in real surfaces. If the in-plane  $|p_x\rangle, |p_y\rangle$  orbitals are also non-negligible, a relevant question here is whether they can influence the orthogonality of the spin and momentum[36, 37, 56]. Including the contribution of these in-plane orbitals, the spin-orbital state is given up to the linear order in  $k$  by,

$$\begin{aligned} |\mathbf{k}\lambda\rangle = & (u_0 - \lambda v_1 k) (|p_z\rangle \otimes |\lambda_\phi\rangle) \\ & - \frac{i}{\sqrt{2}} (\lambda v_0 - u_1 k - w_1 k) (|p_r\rangle \otimes |\lambda_\phi\rangle) \quad (17) \\ & + \frac{1}{\sqrt{2}} (\lambda v_0 - u_1 k + w_1 k) |p_t\rangle \otimes |\bar{\lambda}_\phi\rangle \end{aligned}$$

where  $u_{0,1}, v_{0,1}, w_1$  are material dependent coefficients,  $|\lambda_\phi\rangle = (1/\sqrt{2})[|\uparrow\rangle - \lambda i e^{i\phi}|\downarrow\rangle]$  is the chiral spin-1/2 vortex state,  $|\bar{\lambda}_\phi\rangle = |(-\lambda)_\phi\rangle$  and  $p_r (p_t)$  are the radial (tangential) in-plane combinations of the  $p_x, p_y$ -orbitals given by the  $|p_r(p_t)\rangle = \cos\phi(-\sin\phi)|p_x\rangle + \sin\phi(\cos\phi)|p_y\rangle$ . One may consider that  $||\mathbf{k}\lambda\rangle$  should have been used in this work instead of  $|\mathbf{k}\lambda\rangle$ . Although this is principally correct, the  $||\mathbf{k}\lambda\rangle$  does not change the spin or the spin-momentum orthogonality at the single-particle Hamiltonian level[13, 38]. However, the in-plane orbitals with finite angular momentum states can be coupled by the electron-impurity spin-orbit coupling  $\approx \mathbf{L} \cdot \mathbf{S}$  which play a role in the spin-orbit scattering strength in Eq.(7).

Determination of the constants  $a_{\mathbf{k},\mathbf{k}'}, b_{\mathbf{k},\mathbf{k}'}, c_{\mathbf{k},\mathbf{k}'}$  in Eq.(7) with their full momentum dependence is a fundamentally important problem. Experimentally, the quasi-particle interference (QPI) with spectroscopic STM can be a promising probe of spin-orbit scattering[51, 53]. With this technique the authors in Ref.[51] estimated  $\bar{c} \simeq 80\text{\AA}^2$  for the polar semiconductor *BiTeI*. Here, our discussion on the correlation between electron-impurity scattering and the spin texture provides an alternative method of extracting  $c$  when the warping anisotropy is absent. For a system with inversion symmetry,  $\bar{c}$  can be extracted once the  $\delta_k$  of the spin texture could be measured by using S-ARPES. We know that  $\delta_k \simeq -20^\circ$  in the case of  $\alpha$ -*Sn*[25] and the warping is nearly absent in the surface bands. Using Fig.3, we find that  $\bar{c}/k_F^2 \simeq -40\text{\AA}^2$  putting this material as a strong topological spin-orbit scatterer.

We have shown how spin-orbit scattering from non-magnetic impurities can provide a mechanism for driving deviations from orthogonal spin-momentum locking to produce the NOSML state in strongly spin-orbit coupled materials. Our analysis is based on isotropic electronic bands in systems possessing inversion and time-reversal symmetries and it will be interesting to explore the nature of the NOSML state in more general topological and non-topological systems. Our study highlights the richness of spin textures in spin-orbit coupled materials.

---

\* [hakioglu@itu.edu.tr](mailto:hakioglu@itu.edu.tr)

† These authors contributed equally.

[1] R. Winkler, *Spin-orbit Coupling Effects in Two-Dimensional Electron and Hole Systems*, Springer Tracts in Modern Physics (Springer Berlin Heidelberg, 2003).

[2] M. Dyakonov, *Spin Physics in Semiconductors*, Springer Series in Solid-State Sciences (Springer International Publishing, 2017).

[3] M. Z. Hasan and J. E. Moore, *Annual Review of Condensed Matter Physics* **2**, 55 (2011), <https://doi.org/10.1146/annurev-conmatphys-062910-140432>.

[4] A. Bansil, H. Lin, and T. Das, *Rev. Mod. Phys.* **88**, 021004 (2016).

[5] M. Franz and L. Molenkamp, *Topological Insulators*, ISSN (Elsevier Science, 2013).

[6] F. Ortmann, S. Roche, S. Valenzuela, and L. Molenkamp, *Topological Insulators: Fundamentals and Perspectives* (Wiley, 2015).

[7] S. Hikami, A. I. Larkin, and Y. Nagaoka, *Progress of Theoretical Physics* **63**, 707 (1980), <https://academic.oup.com/ptp/article-pdf/63/2/707/5336056/63-2-707.pdf>.

[8] D. Awschalom, D. Loss, and N. Samarth, *Semiconductor Spintronics and Quantum Computation*, NanoScience and Technology (Springer Berlin Heidelberg, 2013).

[9] O. V. Yazyev, J. E. Moore, and S. G. Louie, *Phys. Rev. Lett.* **105**, 266806 (2010).

[10] A. A. Burkov and D. G. Hawthorn, *Phys. Rev. Lett.* **105**, 066802 (2010).

[11] D. Culcer, E. H. Hwang, T. D. Stanescu, and S. Das Sarma, *Phys. Rev. B* **82**, 155457 (2010).

[12] S. LaShell, B. A. McDougall, and E. Jensen, *Phys. Rev. Lett.* **77**, 3419 (1996).

[13] M. Z. Hasan and C. L. Kane, *Rev. Mod. Phys.* **82**, 3045 (2010).

[14] Z. Jiang, C.-Z. Chang, M. R. Masir, C. Tang, Y. Xu, J. S. Moodera, A. H. MacDonald, and J. Shi, *Nature Communications* **7**, 11458 (2016).

[15] P. Höpfner, J. Schäfer, A. Fleszar, J. H. Dil, B. Slomski, F. Meier, C. Loho, C. Blumenstein, L. Patthey, W. Hanke, and R. Claessen, *Phys. Rev. Lett.* **108**, 186801 (2012).

[16] K. Gotlieb, C.-Y. Lin, M. Serbyn, W. Zhang, C. L. Smallwood, C. Jozwiak, H. Eisaki, Z. Hussain, A. Vishwanath, and A. Lanzara, *Science* **362**, 1271 (2018).

[17] Y. H. Wang, D. Hsieh, D. Pilon, L. Fu, D. R. Gardner, Y. S. Lee, and N. Gedik, *Phys. Rev. Lett.* **107**, 207602 (2011).

[18] S. Basak, H. Lin, L. A. Wray, S.-Y. Xu, L. Fu, M. Z. Hasan, and A. Bansil, *Phys. Rev. B* **84**, 121401 (2011).

[19] C. Howard and M. El-Batanouny, *Phys. Rev. B* **89**, 075425 (2014).

[20] X. Zhu, L. Santos, C. Howard, R. Sankar, F. C. Chou, C. Chamon, and M. El-Batanouny, *Phys. Rev. Lett.* **108**, 185501 (2012).

[21] Z.-H. Pan, A. V. Fedorov, D. Gardner, Y. S. Lee, S. Chu, and T. Valla, *Phys. Rev. Lett.* **108**, 187001 (2012).

[22] R. Heid, I. Y. Sklyadneva, and E. V. Chulkov, *Scientific Reports* **7**, 1095 (2017).

[23] T. Hakioglu, *Phys. Rev. B* **97**, 245145 (2018).

[24] T. Hakioglu, *Phys. Rev. B* **100**, 165407 (2019).

[25] M. R. Scholz, V. A. Rogalev, L. Dudy, F. Reis, F. Adler, J. Aulbach, L. J. Collins-McIntyre, L. B. Duffy, H. F. Yang, Y. L. Chen, T. Hesjedal, Z. K. Liu, M. Hoesch, S. Muff, J. H. Dil, J. Schäfer, and R. Claessen, *Phys. Rev. B* **97**, 075101 (2018).

[26] A. Barfuss, L. Dudy, M. R. Scholz, H. Roth, P. Höpfner, C. Blumenstein, G. Landolt, J. H. Dil, N. C. Plumb, M. Radovic, A. Bostwick, E. Rotenberg, A. Fleszar, G. Bihlmayer, D. Wortmann, G. Li, W. Hanke, R. Claessen, and J. Schäfer, *Phys. Rev. Lett.* **111**, 157205 (2013).

[27] V. A. Rogalev, T. c. v. Rauch, M. R. Scholz, F. Reis, L. Dudy, A. Fleszar, M.-A. Husanu, V. N. Strocov, J. Henk, I. Mertig, J. Schäfer, and R. Claessen, *Phys. Rev. B* **95**, 161117 (2017).

[28] H. Huang and F. Liu, *Phys. Rev. B* **95**, 201101 (2017).

[29] Y. Ohtsubo, P. Le Fèvre, F. m. c. Bertran, and A. Taleb-Ibrahimi, *Phys. Rev. Lett.* **111**, 216401 (2013).

[30] J.-C. Rojas-Sánchez, S. Oyarzún, Y. Fu, A. Marty, C. Vergnaud, S. Gambarelli, L. Vila, M. Jamet, Y. Ohtsubo, A. Taleb-Ibrahimi, P. Le Fèvre, F. Bertran, N. Reyren, J.-M. George, and A. Fert, *Phys. Rev. Lett.* **116**, 096602 (2016).

[31] C.-Z. Xu, Y.-H. Chan, Y. Chen, P. Chen, X. Wang, C. Dejoie, M.-H. Wong, J. A. Hlevyack, H. Ryu, H.-Y. Kee, N. Tamura, M.-Y. Chou, Z. Hussain, S.-K. Mo, and T.-C. Chiang, *Phys. Rev. Lett.* **118**, 146402 (2017).

[32] Q. Barbedienne, J. Varignon, N. Reyren, A. Marty, C. Vergnaud, M. Jamet, C. Gomez-Carbonell, A. Lemaître, P. Le Fèvre, F. m. c. Bertran, A. Taleb-Ibrahimi, H. Jaffrè, J.-M. George, and A. Fert, *Phys. Rev. B* **98**, 195445 (2018).

[33] L. Fu and C. L. Kane, *Phys. Rev. B* **76**, 045302 (2007).

[34] G. Bir and G. Pikus, *Symmetry and Strain-induced Effects in Semiconductors*, A Halsted Press book (Wiley, 1974).

[35] L. Voon and M. Willatzen, *The  $k$   $p$  Method: Electronic Properties of Semiconductors* (Springer Berlin Heidelberg, 2009).

[36] Y. Cao, J. A. Waugh, X.-W. Zhang, J.-W. Luo, Q. Wang, T. J. Reber, S. K. Mo, Z. Xu, A. Yang, J. Schneeloch, G. D. Gu, M. Brahlek, N. Bansal, S. Oh, A. Zunger, and D. S. Dessau, *Nature Physics* **9**, 499 (2013).

[37] H. Zhang, C.-X. Liu, and S.-C. Zhang, *Phys. Rev. Lett.* **111**, 066801 (2013).

[38] L. Fu, *Phys. Rev. Lett.* **103**, 266801 (2009).

[39] H. Mayer and U. Rössler, *Phys. Rev. B* **44**, 9048 (1991).

[40] Q.-Z. Wang, S.-C. Wu, C. Felser, B. Yan, and C.-X. Liu, *Phys. Rev. B* **91**, 165435 (2015).

[41] W. E. Liu, E. M. Hankiewicz, and D. Culcer, *Materials* **10** (2017), 10.3390/ma10070807.

[42] B. Bhattacharyya, B. Singh, R. P. Aloysius, R. Yadav, C. Su, H. Lin, S. Auluck, A. Gupta, T. D. Senguttuvan, and S. Husale, *Scientific Reports* **9**, 7836 (2019).

[43] G. Mahan, *Many-Particle Physics*, Physics of Solids and Liquids (Springer US, 2012).

[44] M. Zhong, S. Li, H.-J. Duan, L.-B. Hu, M. Yang, and R.-Q. Wang, *Scientific Reports* **7**, 3971 (2017).

[45] M. Fischetti and W. Vandenberghe, *Advanced Physics of Semiconductors: Electronic Properties and Transport*, Graduate Texts in Physics (Springer International Publishing, 2016).

[46] S. Ilić, J. S. Meyer, and M. Houzet, *Phys. Rev. Lett.* **119**, 117001 (2017).

[47] N. Mott and H. Massey, *The Theory of Atomic Collisions, by N.F. Mott and H.S.W. Massey. 2nd Edition* (Clarendon Press (printed by C. Batey), 1949).

[48] L. Landau and E. Lifshitz, *Quantum Mechanics: Non-Relativistic Theory*, Teoreticheskaiia fizika (Elsevier Science, 2013).

[49] P. Burke, *Potential Scattering in Atomic Physics* (Springer US, 2012).

[50] H.-A. Engel, B. I. Halperin, and E. I. Rashba, *Phys. Rev. Lett.* **95**, 166605 (2005).

[51] Y. Kohsaka, T. Machida, K. Iwaya, M. Kanou, T. Hanaguri, and T. Sasagawa, *Phys. Rev. B* **95**, 115307 (2017).

[52] W.-Y. Shan, H.-Z. Lu, and S.-Q. Shen, *Phys. Rev. B* **86**, 125303 (2012).

[53] W.-C. Lee, C. Wu, D. P. Arovas, and S.-C. Zhang, *Phys. Rev. B* **80**, 245439 (2009).

[54] See the supplementary material of this manuscript.

[55] A. V. Balatsky, I. Vekhter, and J.-X. Zhu, *Rev. Mod. Phys.* **78**, 373 (2006).

[56] J. H. Dil, *Electronic Structure* **1**, 023001 (2019).

## Supplementary Material: Non-orthogonal spin-momentum locking

T. Hakioglu <sup>†, 1, 2, \*</sup> Wei-Chi Chiu,<sup>2, †</sup> R. S. Markiewicz,<sup>2</sup> Bahadur Singh,<sup>3</sup> and A. Bansil<sup>2</sup>

<sup>1</sup>*Energy Institute and Department of Physics, Istanbul Technical University  
Maslak 34469, Istanbul, Turkey*

<sup>2</sup>*Department of Physics, Northeastern University, Boston, MA 02115, USA*

<sup>3</sup>*Department of Condensed Matter Physics and Materials Science,  
Tata Institute of Fundamental Research, Colaba, Mumbai 400005, India*

Here we discuss details of the impurity averaging of the electron self-energy and the Green's function. Diagrammatically the electron-impurity interaction is described by the Feynman diagrams as shown in Fig.(1).

We consider that the impurity at the random position  $\mathbf{R}_i$  is scattered by electrons with initial and final momenta  $\mathbf{k}, \mathbf{k}'$ . By the impurity averaging we mean a two-step process. The first is that the kinetic phase  $e^{i(\mathbf{k}-\mathbf{k}') \cdot \mathbf{R}_i}$  of the electron wavefunction acquired at the  $i$ 'th scattering is randomized by the random position  $\mathbf{R}_i$  of the  $i$ 'th impurity. This leads to the average over the impurity positions as described in a separate section below. The second crucial factor is that the random impurity positions also lead to randomized incidence direction of the electron between two scattering events. In order to avoid averaging over the random initial-final momentum orientations at each scattering, we must form scalar quantities of the self-energy vector as  $\Sigma_k = \Sigma \cdot \hat{\mathbf{k}}$  and  $\Sigma_g = \Sigma \cdot \hat{\mathbf{g}}_k$  as the component of the self-energy along the momentum and along the spin-orbit vector. The  $\Sigma_k$  and  $\Sigma_g$  are scalar quantities which are not affected by the random directions of the initial state vector  $\mathbf{k}$  before each scattering.

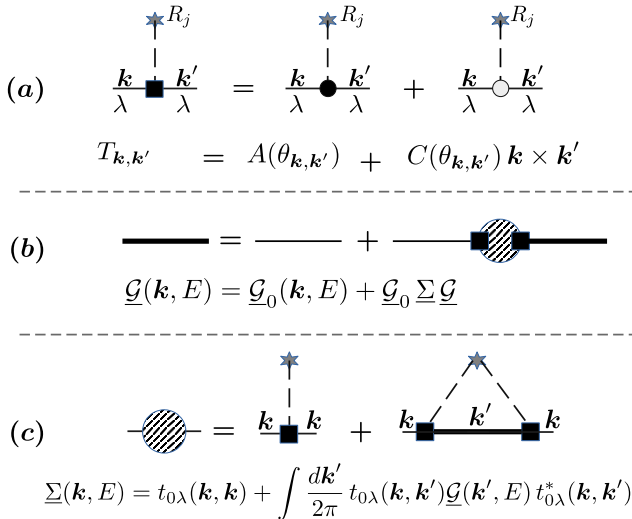


FIG. 1. Feynman diagrams corresponding to the first order electron-impurity vertex (a), the Green's function (b) and the electron self-energy (c).

### Averaging over impurity positions

We define the average over the impurity positions by

$$\langle O \rangle_{imp} = \int d\mathbf{R} O(\mathbf{R}) P(\mathbf{R}) \quad (1)$$

Here  $P(\mathbf{R})$  is the classical distribution of the impurity positions and  $O(\mathbf{R})$  is a generic quantity to be averaged. In our case the impurity positions are completely random with  $P(\mathbf{R}) = 1/\Omega$  with  $\Omega$  being the area in which the impurities are randomly scattered.

Considering that the impurity-electron interaction is weak, we use a perturbative expansion of the electron Green's function including the first and second order terms in the impurity-electron scattering matrix elements  $T_0(\mathbf{k}, \mathbf{k}')$ . The full self-energy is given in Eq.(8) of the main text. The impurity average of the self-energy is:

$$\begin{aligned} \langle \Sigma(\mathbf{k}, E) \rangle_{imp} &= \langle T_0(\mathbf{k}, \mathbf{k}) \rangle_{imp} \\ &+ \int \frac{d\mathbf{k}'}{2\pi} \langle T_0(\mathbf{k}, \mathbf{k}') \underline{\mathcal{G}}(\mathbf{k}', E) T_0^*(\mathbf{k}, \mathbf{k}') \rangle_{imp} \end{aligned} \quad (2)$$

where the scattering matrix  $T_0(\mathbf{k}, \mathbf{k}')$  has been derived in the following section in Eq.(22) as

$$T_{0\lambda}(\mathbf{k}, \mathbf{k}') = \sum_{j=1}^{N_{imp}} e^{i(\mathbf{k}-\mathbf{k}') \cdot \mathbf{R}_j} t_{0\lambda}^{(j)}(\mathbf{k}, \mathbf{k}') \quad (3)$$

with the  $j$ -index in the summation describing the  $j$ 'th impurity. The Feynman diagrams corresponding to the  $t_{0\lambda}^{(j)}(\mathbf{k}, \mathbf{k}')$  are shown in Fig.(1.a). In Eq.(2) the  $\underline{\mathcal{G}}(\mathbf{k}', E)$  is the interacting electron Green's function in the  $2 \times 2$ -matrix form in the electron-spin space as described by the Dyson equation

$$\frac{1}{\underline{\mathcal{G}}(\mathbf{k}, E)} = \frac{1}{\underline{\mathcal{G}}_0(\mathbf{k}, E)} - \underline{\Sigma}(\mathbf{k}, E) \quad (4)$$

with

$$\underline{\mathcal{G}}_0(\mathbf{k}, E) = \frac{1}{E - \xi_{\mathbf{k}} - \mathbf{g}_{\mathbf{k}} \cdot \boldsymbol{\sigma}} \quad (5)$$

representing the non-interacting Green's function and the  $\underline{\Sigma}(\mathbf{k}, E) = \Sigma_0(\mathbf{k}, E) \sigma_0 + \Sigma(\mathbf{k}, E) \cdot \boldsymbol{\sigma}$  the full electron self-energy. The  $\underline{\mathcal{G}}(\mathbf{k}, E)$  can be compactly written as

$$\underline{\mathcal{G}}(\mathbf{k}, E) = \frac{1}{2} \sum_{\lambda} [1 + \lambda \hat{\mathbf{G}}(\mathbf{k}, E) \cdot \boldsymbol{\sigma}] \mathcal{G}^{(\lambda)}(\mathbf{k}, E) \quad (6)$$

with

$$\mathcal{G}^{(\lambda)}(\mathbf{k}, E) = \frac{1}{E - E_{\mathbf{k}}^{\lambda}} \quad (7)$$

as the exact Green's function of the quasiparticles in the spin-orbit eigenband  $\lambda$ . The  $\mathbf{G}(\mathbf{k}, E) = \mathbf{g}_{\mathbf{k}} + \Sigma(\mathbf{k}, E)$  is the renormalized spin-orbit vector and  $\hat{\mathbf{G}}$  is the unit vector of  $\mathbf{G}$ . Eq.(6) is the direct sum of the contributions from each spin-orbit band singled out by the physical pole-position of the  $\mathcal{G}^{(\lambda)}(\mathbf{k}, E)$  at  $E = E_{\mathbf{k}}^{\lambda}$ .

We turn now examine the full self-energy in Eq.(2) diagrammatically. The first term  $\langle T_0(\mathbf{k}, \mathbf{k}') \rangle_{imp}$  is the impurity average in Eq.(3) for which we use:

$$\sum_{j=1}^{N_{imp}} \langle e^{i(\mathbf{k}-\mathbf{k}') \cdot \mathbf{R}_j} \rangle_{imp} = \frac{1}{\Omega} \int d^3 \mathbf{R} \sum_{j=1}^{N_{imp}} e^{i(\mathbf{k}-\mathbf{k}') \cdot \mathbf{R}} = n_{imp} \delta_{\mathbf{k}, \mathbf{k}'} \quad (8)$$

as depicted in Fig.(1.a). Here,  $n_{imp} = N_{imp}/\Omega$  is the average impurity concentration.  $\langle T_0(\mathbf{k}, \mathbf{k}') \rangle_{imp} = N_i \delta_{\mathbf{k}, \mathbf{k}'} t_{0\lambda}(\mathbf{k}, \mathbf{k})$ . The main effect of this term is to shift the Fermi energy by a constant and not contribute to the energy-spin renormalization. The impurity average in the second term in Eq.(2) includes  $\langle T_0 \underline{\mathcal{G}} T_0^* \rangle_{imp}$ , which requires the knowledge of the full Green's function. Here, we replace the full Green's function  $\underline{\mathcal{G}}$  by the non-interacting one  $\underline{\mathcal{G}}_0$  as given by Eq.(5), which yields the exact result in the electron self-energy up to second order in electron-impurity coupling as mentioned before Eq.(2). The result is,

$$\langle T_0 \underline{\mathcal{G}}(\mathbf{k}', E) T_0^\dagger \rangle_{imp} \simeq \frac{1}{\Omega} \sum_{i,j} \langle e^{i(\mathbf{k}-\mathbf{k}') \cdot (\mathbf{R}_i - \mathbf{R}_j)} \rangle_{imp} \times t_0(\mathbf{k}, \mathbf{k}') \underline{\mathcal{G}}_0(\mathbf{k}', E) t_0^*(\mathbf{k}, \mathbf{k}') \quad (9)$$

where the part depending on the impurity average is by definition

$$\begin{aligned} \sum_{i,j} \langle e^{i(\mathbf{k}-\mathbf{k}') \cdot (\mathbf{R}_i - \mathbf{R}_j)} \rangle_{imp} &= \frac{1}{\Omega} \sum_{i=j} 1 \\ &+ \sum_{i \neq j} \langle e^{i(\mathbf{k}-\mathbf{k}') \cdot (\mathbf{R}_i - \mathbf{R}_j)} \rangle_{imp} \end{aligned} \quad (10)$$

The impurity averaging over a totally random impurity distribution yields random interference between different impurities when  $\mathbf{R}_i \neq \mathbf{R}_j$  yielding a vanishing contribution for  $\mathbf{k}' \neq \mathbf{k}$ . This term is therefore (with  $1 \ll N_{imp}$ )

$$\sum_{i \neq j} \langle e^{i(\mathbf{k}-\mathbf{k}') \cdot (\mathbf{R}_i - \mathbf{R}_j)} \rangle_{imp} = n_{imp}^2 \delta_{\mathbf{k}, \mathbf{k}'} \quad (11)$$

Hence it averages out to zero when  $\mathbf{k} \neq \mathbf{k}'$  like the first order impurity average in Eq.(8). The net effect of this term is therefore essentially the same as the first order impurity-vertex. The net effect of the impurity averaging

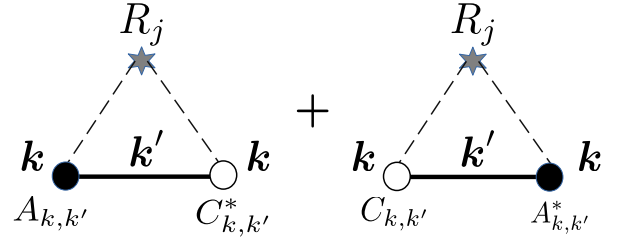


FIG. 2. Second order Feynman diagrams for the self-energy contributing to the NOSML. These terms have linear dependence on the spin-orbit scattering strength  $C_{k,k'}$ . The solid line represents the bare electron propagator, and the dashed line represents the two scattering events with the impurity  $R_j$ . (The second order contributions in  $A_{k,k'}$  and  $C_{k,k'}$  do not contribute significantly to the NOSML and therefore omitted in this picture.)

in Eq.(10) is therefore provided by the first term on the right hand side as  $(1/\Omega) \sum_i 1 = n_{imp}$ . Eq.(9) is therefore given by

$$\langle T_0 \underline{\mathcal{G}} T_0^* \rangle_{imp} = n_{imp} t_0(\mathbf{k}, \mathbf{k}') \underline{\mathcal{G}}_0(\mathbf{k}', E) t_0^*(\mathbf{k}, \mathbf{k}') \quad (12)$$

Using this result in Eq.(2) we find

$$\langle \Sigma(\mathbf{k}, E) \rangle_{imp} \simeq n_i \int \frac{d\mathbf{k}'}{2\pi} |t_0(\mathbf{k}, \mathbf{k}')|^2 \underline{\mathcal{G}}_0(\mathbf{k}', E) \quad (13)$$

writing  $\underline{\mathcal{G}}_0(\mathbf{k}', E)$  similarly to the Eq.(6)

$$\underline{\mathcal{G}}_0(\mathbf{k}, E) = \frac{1}{2} \sum_{\lambda} [1 + \lambda \hat{\mathbf{g}}_{\mathbf{k}} \cdot \boldsymbol{\sigma}] \mathcal{G}_0^{(\lambda)}(\mathbf{k}, E) \quad (14)$$

from which, the components of the self-energy are found to be  $\langle \Sigma_0 \rangle_{imp} = \sum_{\lambda} \langle \Sigma_0^{(\lambda)} \rangle_{imp}$  and  $\langle \Sigma \rangle_{imp} = \sum_{\lambda} \langle \Sigma^{(\lambda)} \rangle_{imp}$  where we used the Eqs. (9) in the main text. The result is,

$$\langle \Sigma_0^{(\lambda)} \rangle_{imp} = \frac{n_i}{2} \int \frac{d\mathbf{k}'}{2\pi} |t_0(\mathbf{k}, \mathbf{k}')|^2 \mathcal{G}_0^{(\lambda)}(\mathbf{k}, E) \quad (15)$$

$$\langle \Sigma^{(\lambda)} \rangle_{imp} = \lambda \frac{n_i}{2} \int \frac{d\mathbf{k}'}{2\pi} |t_0(\mathbf{k}, \mathbf{k}')|^2 \hat{\mathbf{G}}_0^{(\lambda)}(\mathbf{k}', E) \mathcal{G}_0^{(\lambda)}(\mathbf{k}', E) \quad (16)$$

These are the self-energy expressions obtained from Eq.(8) in the manuscript.

Next we consider the second type of average which is due to the random orientations of the initial/final momenta. The vectorial SDSE  $\langle \Sigma^{(\lambda)} \rangle_{imp}$  as defined in Eqs.

(16) is not a meaningful average due to the fact that, at every scattering, the direction of  $\langle \Sigma^{(\lambda)} \rangle_{imp}$  is randomized by the random directions of  $\mathbf{k}$  vectors. However,  $\Sigma_k = \langle \Sigma^{(\lambda)} \cdot \hat{\mathbf{k}} \rangle_{imp}$  and  $\Sigma_g = \langle \Sigma^{(\lambda)} \cdot \hat{\mathbf{g}}_{\mathbf{k}} \rangle_{imp}$  are meaningful quantities to consider in this case since both are scalars and unaffected by the random directions of the scattered electron momenta. Indeed, the complex scalar form  $\mathcal{S}_k^{\lambda} = \Sigma_g + i \Sigma_k$  is well suited for this purpose. After a similar calculation to the Eqs. (16) above, we easily calculate the  $\mathcal{S}_k^{\lambda}$  as shown in Eq.(13) of the manuscript.

### THE SCATTERING MATRIX $t_{0\lambda}(\mathbf{k}, \mathbf{k}')$

Here we examine the time reversal and other symmetry properties of  $t_{0\lambda}(\mathbf{k}, \mathbf{k}')$  in Eq.(7) of the manuscript in the presence of spin-orbital scattering.

The full electron-impurity potential  $V_{ei}(\mathbf{r})$  is the sum of all electron-impurity potentials localized at the impurity positions  $\mathbf{R}_i$  as

$$V_{ei}(\mathbf{r}) = \sum_{i=1}^{N_{imp}} v_{ei}^{(i)}(\mathbf{r} - \mathbf{R}_i) \quad (17)$$

where  $N_{imp}$  is the total number of impurities.  $v_{ei}^{(i)}(\mathbf{r})$  is a sum of the spin independent and the spin-orbit scattering potentials  $v_0^{(i)}$  and  $v_{so}^{(i)}$ , respectively as

$$v_{ei}^{(i)}(\mathbf{r}) = v_0^{(i)}(\mathbf{r}) + v_{so}^{(i)}(\mathbf{r}), \quad \text{where} \quad (18)$$

$$v_{so}^{(i)}(\mathbf{r}) = \sigma \cdot [\nabla v_0^{(i)}(\mathbf{r}) \times \mathbf{p}] \quad (19)$$

We consider only one type of impurity and assume that  $v_{ei}^{(i)}$  is the same for all impurities. The general quantum state of the Bloch electrons is given by

$$\langle \mathbf{r} | \mathbf{k} \lambda \rangle = e^{i \mathbf{k} \cdot \mathbf{r}} u_{\mathbf{k}}^{(\lambda)}(\mathbf{r}) \quad (20)$$

with  $u_{\mathbf{k}}^{(\lambda)}(\mathbf{r})$  carrying information about the orbital symmetries of the  $\lambda$  band. Dropping the index  $i$  in  $v_0^{(i)}$ , the intra-band scattering amplitude is given by

$$\begin{aligned} T_{0\lambda}(\mathbf{k}, \mathbf{k}') &= \langle \mathbf{k}' \lambda | V_{ei} | \mathbf{k} \lambda \rangle \\ &= \int d\mathbf{r} e^{i(\mathbf{k}-\mathbf{k}') \cdot \mathbf{r}} u_{\mathbf{k}'}^{(\lambda)*}(\mathbf{r}) V_{ei}(\mathbf{r}) u_{\mathbf{k}}^{(\lambda)}(\mathbf{r}) \end{aligned} \quad (21)$$

Inserting Eq.(17) into Eq.(21), we find,

$$T_{0\lambda}(\mathbf{k}, \mathbf{k}') = \sum_i e^{i(\mathbf{k}-\mathbf{k}') \cdot \mathbf{R}_i} t_{0\lambda}(\mathbf{k}, \mathbf{k}') \quad (22)$$

where

$$t_{0\lambda}(\mathbf{k}, \mathbf{k}') = \tilde{v}_0(\mathbf{k}, \mathbf{k}') + \tilde{v}_{so}(\mathbf{k}, \mathbf{k}') \quad (23)$$

with

$$\tilde{v}_0(\mathbf{k}, \mathbf{k}') = \int d\mathbf{r} e^{i(\mathbf{k}-\mathbf{k}') \cdot \mathbf{r}} u_{\mathbf{k}'}^{(\lambda)*}(\mathbf{r}) v_0(\mathbf{r}) u_{\mathbf{k}}^{(\lambda)}(\mathbf{r}) \quad (24)$$

$$\tilde{v}_{so}(\mathbf{k}, \mathbf{k}') = \int d\mathbf{r} e^{i(\mathbf{k}-\mathbf{k}') \cdot \mathbf{r}} u_{\mathbf{k}'}^{(\lambda)*}(\mathbf{r}) v_{so}(\mathbf{r}) u_{\mathbf{k}}^{(\lambda)}(\mathbf{r})$$

Eqs.(21)-(24) comprise a generic derivation of Eq.(6) in the main text.

This general formulation can be applied to specific cases only when the Bloch state in Eq.(20) and the electron-impurity potential  $v_0(\mathbf{r})$  are known. However, we can still say more about the  $t_{0\lambda}(\mathbf{k}, \mathbf{k}')$  using the fundamental symmetries that it must respect. These are,

1. the time reversal symmetry:  $t_{0\lambda}(\mathbf{k}, \mathbf{k}') = t_{0\bar{\lambda}}^*(-\mathbf{k}', -\mathbf{k})$ ,
2. the unitarity of the scattering matrix elements:  $t_{0\lambda}(\mathbf{k}, \mathbf{k}') = t_{0\lambda}^*(\mathbf{k}', \mathbf{k})$  and
3. invariance under in-plane rotations:  $t_{0\lambda}(R_{\Lambda} : \mathbf{k}, R_{\Lambda} : \mathbf{k}') = t_{0\lambda}(\mathbf{k}, \mathbf{k}')$  where  $R_{\Lambda}$  is the rotation operator by an angle  $\Lambda$  in the plane of the general non-collinear vectors  $\mathbf{k}, \mathbf{k}'$ .

We write a minimal form satisfying these conditions as

$$t_{0\lambda}(\mathbf{k}, \mathbf{k}') = a_{\lambda}(k, k') + b_{\lambda}(k, k') \hat{\mathbf{k}} \cdot \hat{\mathbf{k}}' + c_{\lambda}(k, k') \hat{\mathbf{k}} \times \hat{\mathbf{k}}' \cdot \hat{\mathbf{e}}_z \quad (25)$$

where  $\hat{\mathbf{k}} \cdot \hat{\mathbf{k}}' = \cos(\phi - \phi')$  and  $\hat{\mathbf{k}} \times \hat{\mathbf{k}}' \cdot \hat{\mathbf{e}}_z = \sin(\phi - \phi')$ . The coefficients  $a_{\lambda}(k, k')$ ,  $b_{\lambda}(k, k')$  and  $c_{\lambda}(k, k')$  are the  $s$ -wave,  $p$ -wave and the spin-orbit scattering strengths which depend on the electron-impurity interaction and the quantum state of the electrons and the impurity. These three scattering channels are generally the most fundamental ones present in a large number of strongly spin-orbit coupled materials. The unitarity condition is

$$\begin{aligned} a_{\lambda}(k, k') &= a_{\lambda}^*(k', k) \\ b_{\lambda}(k, k') &= b_{\lambda}^*(k', k) \\ -c_{\lambda}(k, k') &= c_{\lambda}^*(k', k) . \end{aligned} \quad (26)$$

On the other hand, time-reversal symmetry requires that

$$\begin{aligned} a_{\lambda}(k, k') &= a_{\lambda}^*(k', k) \\ b_{\lambda}(k, k') &= b_{\lambda}^*(k', k) \\ -c_{\lambda}(k, k') &= c_{\lambda}^*(k', k) . \end{aligned} \quad (27)$$

Their combined effect is that the coefficients in this simplest general form are independent of  $\lambda$ . Dropping the  $\lambda$  index, the NOSML is a result of the non-zero  $\mathcal{C} = \text{Re}\{a(k, k')c^*(k, k')\}$  in the scattering intensity  $|t_0(\mathbf{k}, \mathbf{k}')|^2$ . Using this result, we finally find that

$$\begin{aligned} T_{0\lambda}(k, k') &= \frac{1}{|a|^2} \int \frac{d\theta_{\mathbf{k}, \mathbf{k}'}}{2\pi} \left| t_0(\mathbf{k}, \mathbf{k}') \right|^2 e^{-i\theta_{\mathbf{k}, \mathbf{k}'}} \\ &\simeq 1 + \text{Re}\{ab^*\} + i \text{Re}\{ac^*\} \end{aligned} \quad (28)$$

where we assumed that  $|b| \ll |a|$  and  $|c| \ll |a|$  and ignored the second order terms in  $b$  and  $c$ . Eq.(28) is the same as Eq.(14) in the main text.

\* [hakioglu@itu.edu.tr](mailto:hakioglu@itu.edu.tr)

† These authors contributed equally.